JACS
JOURNAL OF THE AMERICAN CHEMICAL SOCIETY
Article
pubs.acs.org/JACS

Zn−Cu−In−Se Quantum Dot Solar Cells with a Certified Power Conversion Efficiency of 11.6%

Jun Du,[†,▽] Zhonglin Du,[†,▽] Jin-Song Hu,[§,▽] Zhenxiao Pan,[†] Qing Shen,[∥,⊥] Jiankun Sun,[§] Donghui Long,[‡] Hui Dong,[#] Litao Sun,[#] Xinhua Zhong,[*,†] and Li-Jun Wan[§]

[†]Key Laboratory for Advanced Materials, Institute of Applied Chemistry, and [‡]School of Chemical Engineering, East China University of Science and Technology, Shanghai 200237, China

[§]Beijing National Laboratory for Molecular Sciences, Key Laboratory of Molecular Nanostructure and Nanotechnology, Institute of Chemistry, Chinese Academy of Sciences, University of Chinese Academy of Sciences, Beijing 100190, China

[∥]Department of Engineering Science, University of Electro-Communications, Tokyo 182-8585, Japan

[⊥]Japan Science and Technology Agency (JST), Saitama 332-0012, Japan

[#]SEU FEI Nanopico Center, Key Lab of MEMS of Ministry of Education, Southeast University, Nanjing 210096, China

Supporting Information

ABSTRACT: The enhancement of power conversion efficiency (PCE) and the development of toxic Cd-, Pb-free quantum dots (QDs) are critical for the prosperity of QD-based solar cells. It is known that the properties (such as light harvesting range, band gap alignment, density of trap state defects, etc.) of QD light harvesters play a crucial effect on the photovoltaic performance of QD based solar cells. Herein, high quality ∼4 nm Cd-, Pb-free Zn−Cu−In−Se alloyed QDs with an absorption onset extending to ∼1000 nm were developed as effective light harvesters to construct quantum dot sensitized solar cells (QDSCs). Due to the small particle size, the developed QD sensitizer can be efficiently immobilized on TiO_2 film electrode in less than 0.5 h. An average PCE of 11.66% and a certified PCE of 11.61% have been demonstrated in the QDSCs based on these Zn−Cu−In−Se QDs. The remarkably improved photovoltaic performance for Zn−Cu−In−Se QDSCs vs Cu−In−Se QDSCs (11.66% vs 9.54% in PCE) is mainly derived from the higher conduction band edge, which favors the photogenerated electron extraction and results in higher photocurrent, and the alloyed structure of Zn−Cu−In−Se QD light harvester, which benefits the suppression of charge recombination at photoanode/electrolyte interfaces and thus improves the photovoltage.

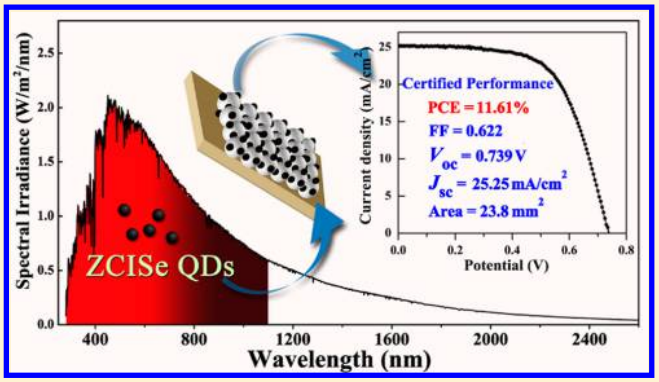

INTRODUCTION

Colloidal quantum dots (QDs) are extremely appealing light harvesters for photovoltaic (PV) applications owing to their excellent optoelectronic properties such as high absorption coefficient, tunable band gap, multiple exciton generation possibility, solution processability, as well as facile and low-cost availability.[1−5] These properties result in the recent promising progress for QD based PV devices (including both QD sensitized solar cells (QDSCs) and depleted heterojunction solar cells) with best power conversion efficiencies (PCE) over 9%.[6−9] However, most of the reported QD based solar cells contain highly toxic Cd or Pb elements, which may limit their commercial applications in consideration of environmental and health concerns. Therefore, the development of efficient and heavy-metal free QD light absorbers is critical for the practical applications of QD based solar cells.[10]

Less-toxic I−III−VI_2 group QDs, especially $CuInS_2$ (CIS) and $CuInSe_2$ (CISe) QDs, with high absorption coefficient (∼10^5 cm^{-1}) and near optimal band gap energy (1.0−1.5 eV) are attractive alternatives to the highly toxic cadmium and lead chalcogenide QDs.[11,12] Pioneering work with promising results has been performed in exploring CIS and CISe QDs for PV applications.[13−24] The PCEs of CIS based QDSCs have been improved steadily from less than 1% to ∼5% through the interfacial engineering by introducing buffer layer between QD sensitizers and electron acceptor TiO_2,[13−17] or band gap engineering with use of cosensitization strategy.[16−23] Very recently, significant progress has been achieved for CIS QDSCs by the overgrowth of wide band gap ZnS shell around CIS QDs to form quasi type-I core/shell structured CIS/ZnS QDs for eliminating surface trapping defects, which resulted in a certified PCE of 6.66%.[24] Compared to CIS QDs, CISe QDs are more promising light harvesters due to a larger exciton Bohr

Received: January 18, 2016
Published: March 10, 2016

DOI: 10.1021/jacs.6b00615
J. Am. Chem. Soc. 2016, 138, 4201−4209

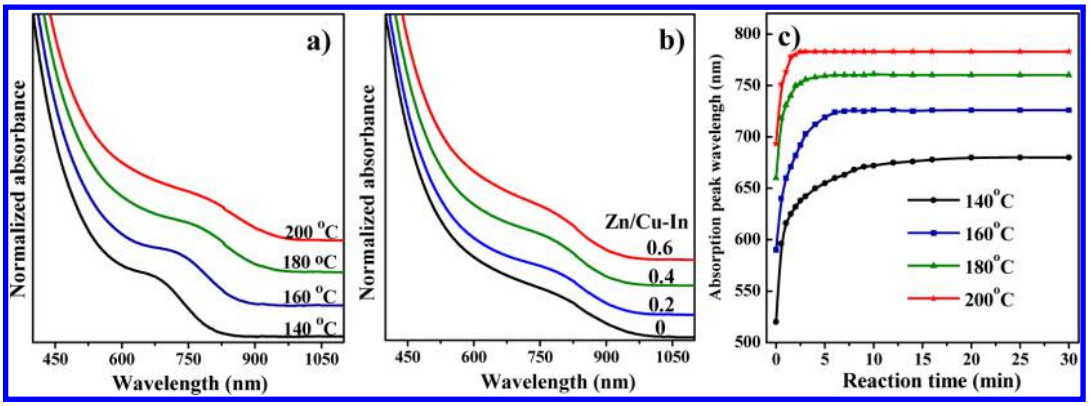

Figure 1. Absorption spectra of Zn−Cu−In−Se QDs synthesized under (a) different temperatures with a fixed Zn/Cu−In ratio at 0.4; (b) different Zn/Cu−In ratios with a constant temperature at 200 °C. (c) Temporal evolution of excitonic absorption peak positions for the Zn−Cu−In−Se QDs synthesized at different temperatures with a fixed Zn/Cu−In ratio of 0.4.

radius (10.6 vs 4.1 nm) and a narrower bulk band gap energy (1.04 vs 1.5 eV), which enable the light absorption edge to extend to near-infrared (NIR) region to better match the solar spectrum.[25] To expand the light-harvesting range and improve PCE, especially the photocurrent of a QDSC, $CuInSe_{1-x}S_x$ alloyed QDs were therefore developed by Klimov et al. to achieve a QDSC with a PCE of 5.5%.[26,27] CISe QD based heterojunction solar cells have been also demonstrated by Korgel and co-workers.[28−30] It is noted that in the process of this manuscript preparation, Hyeon et al. optimized the thickness of ZnS barrier layer in CISe QDSCs and obtained a record high PCE of 8.1% for Cd-, Pb-free QD solar cells.[31,32] Up to date, however, the PCEs of either CIS or CISe based QDSCs still lag behind those of highly toxic cadmium chalcogenide QD based QDSCs.[6,7,33]

The mean performance of CIS and CISe based QDSCs is partially limited by the high density of trap state defects in these QDs, which usually serve as charge recombination centers and thus deteriorate the photovoltaic performance, especially the photovoltage.[24,27,28,34,35] In order to minimize trap state defects, overcoating subnanometer thick wide band gap ZnS shell on CIS QDs to form quasi type-I core/shell structure,[24] or depositing 2−3 nm thick ZnS barrier layer on CISe sensitized photoanode has been applied to achieve remarkable improvement on the photovoltaic performance.[31,32,36] Contrasting to the core/shell structured QD sensitizers, where the wide band gap shell layer has two conflicting effects: reducing surface trapping defects and therefore favoring charge recombination control, but retarding electron injection and hole scavenge simultaneously,[7,24] alloyed QD sensitizers instead could not only improve the chemical stability and reduce the density of trapping defects due to the hardened lattice structure and decreased atomic intradiffusion, but also favor the electron injection due to the upshift of conduction band edge.[37,38] Therefore, alloyed QDs could outperform the type-I core/shell structured QDs in serving as light-harvesting sensitizers in QDSCs. The successful application of alloyed QDs as light-harvesting sensitizers in QDSCs has been seen in several examples such as $CdSe_xTe_{1-x}$,[6,33,39] $CuInSe_xS_{1-x}$,[26,27] and $(CISe)_{1-x}(ZnS)_x$ QDs,[36] among which a PCE up to 9% has been achieved.[6]

In this work, we target at constructing high efficiency QDSCs based on Zn−Cu−In−Se alloyed QD light harvesters. High quality oleylamine capped Zn−Cu−In−Se QDs with absorption onset extending to ∼1000 nm were synthesized via alloying CISe and ZnSe constituents in the nucleation and growth of QDs at high temperature, followed by a ligand exchange process to obtain a bifunctional linker (mercaptopropionic acid (MPA)) capped water-soluble QDs. The obtained water-soluble MPA-capped QDs were then tethered on mesoporous TiO_2 film electrode via the capping ligand induced self-assembly approach by pipetting QD aqueous solutions onto the film electrode. Benefiting from the high QD loading and intrinsic superior optoelectronic properties of the Zn−Cu−In−Se alloyed QD sensitizer (broad light-harvesting range, high electron injection rate, suppressed charge recombination kinetics, etc.), the resulting Cd-, and Pb-free QDSCs exhibited a champion PCE of 11.91% and a certified PCE of 11.61% under 1 full sun illumination, which is the world-record performance for all kinds of QD solar cells up to now.[6−9]

RESULTS AND DISCUSSION

Synthesis and Optoelectronic Properties of Zn−Cu−In−Se QD Sensitizers. Dodecanethiol (DDT) is commonly used as a capping ligand in the synthesis of I−III−VI_2 QDs.[40−43] Unfortunately, DDT-capped QDs usually lead to low QD loading and poor photovoltaic performance in the resultant cell devices since the initial DDT ligand cannot be completely replaced by other bifunctional ligands.[23,26,44] Therefore, a DDT-free synthetic approach was developed in this work. Zn−Cu−In−Se alloyed QDs were synthesized via a facile one-pot approach using the reaction of diphenylphosphine selenide (DPP-Se) with a mixture of cation precursors (CuI, $In(OAc)_3$, and $Zn(OAc)_2$) in oleylamine media at high temperature according to a modified literature method.[28] The Zn−Cu−In−Se QDs were formed via a "simultaneous nucleation and growth" strategy. In the synthesis, the molar ratio for Cu, In, and Se precursors was fixed at 1:1:3, and the amount of Zn precursor was variable. The detailed synthetic procedure is described in the Experimental Section. The use of highly reactive DPP-Se anion precursor enabled the successful synthesis of Zn−Cu−In−Se QDs with no need of conventional DDT ligand.

Through this synthetic approach, the absorption onsets of the obtained Zn−Cu−In−Se QDs can be conveniently tuned by varying the reaction temperature and reactant composition (i.e., Zn/Cu−In ratio). Experimental results indicate that under a fixed reactant composition (Zn/Cu−In = 0.4), the absorption onset of the obtained QDs can be tuned from 860 to 980 nm as

DOI: 10.1021/jacs.6b00615
J. Am. Chem. Soc. 2016, 138, 4201−4209

the increase of reaction temperature from 140 to 200 °C (Figure 1a). Since precipitation occurred in the reaction system when the reaction temperature was over 200 °C, the up-limit of the reaction temperature was set at 200 °C. Moreover, under a constant reaction temperature at 200 °C, as the nominal Zn/Cu−In ratio was increased from 0 to 0.6, the absorption onset varied from 1060 to 960 nm (Figure 1b). Unlike the situation for some ternary and quaternary semiconductor QDs with a poorly resolved excitonic absorption peak,[40−43] a relatively sharp and distinct excitonic absorption peak can be observed in the absorption spectrum of each sample prepared at different synthetic conditions in our case. This indicates a homogeneous distribution of the composition, size and shape of the obtained particles. The corresponding band gaps of these QDs were then determined by the corresponding excitonic absorption peak positions and the detailed results are shown in Table S1 in the Supporting Information (SI). It should be noted that due to the existence of extended tail absorption arising from the intra band states,[12] the obtained band gap energy in wavelength unit is remarkably shorter than the corresponding absorption onset. Another advantage of this synthetic approach is that a fast growth kinetics (<4 min) followed by a long-term plateau stage (>30 min) for the excitonic peak position is observed (Figure 1c). This indicates that the target Zn−Cu−In−Se QDs can be formed very quickly and the chemical composition and size of the formed QDs can remain constant for a long period. The inherent mechanism for this phenomenon can be ascribed to hardened structure in the formed alloyed QDs, as observed in previous reports.[38] These results indicates that the developed synthetic approach is timesaving and highly reproducible.

The successful incorporation of ZnSe constituent into CISe host was confirmed by the inductively coupled plasma-atomic emission spectrometry (ICP-AES) measurements. The detailed results are available in Table S2. The measured Zn/Cu/In molar ratio is close to the nominal Zn/Cu/In ratio used in the synthesis. The obtained chemical composition of Zn−Cu−In−Se QDs is consistent with the stoichiometric ratio of $(CuInSe_2)_x(ZnSe)_{1-x}$. Wide-angle X-ray diffraction (XRD) patterns (Figure 2a) of the representative Zn−Cu−In−Se QD samples with nominal Zn/Cu−In ratio of 0, 0.4, and 0.6 exhibit characteristic diffraction patterns for chalcopyrite structure (JCPDS: no. 40−1487). With the increase of Zn/Cu−In ratio from 0 to 0.6, the peak positions shifted steadily from chalcopyrite $CuInSe_2$ to zinc blend ZnSe, indicating the formation of alloyed QDs. Meanwhile, the consecutive blue-shift observed in the excitonic peak positions with the increase of Zn content as shown in Figure 1b gives further support to the alloyed structure of the obtained Zn−Cu−In−Se QDs. This is because a core/shell structure would cause the red-shift of excitonic peak positions.[38] Since the focus of this work is the PV applications of the obtained QDs, no further structural characterizations were performed on the obtained alloyed QDs at this stage.

The photovoltaic performances of QDSCs based on Zn−Cu−In−Se QDs synthesized under different conditions were first evaluated and shown in Tables S3 and S4 as well as in Figures S1 and S2. These results indicate that the $(CISe)_{0.7}$-$(ZnSe)_{0.3}$ QDs synthesized under a nominal Zn/Cu−In ratio of 0.4 and reaction temperature of 200 °C delivered the best performance with an average PCE of 11.66 ± 0.17%. For convenience, ZCISe QDs are referred specially to $(CISe)_{0.7}$-$(ZnSe)_{0.3}$ QDs henceforth; and the QDSCs based on this QD sensitizer were further studied and compared to the reference

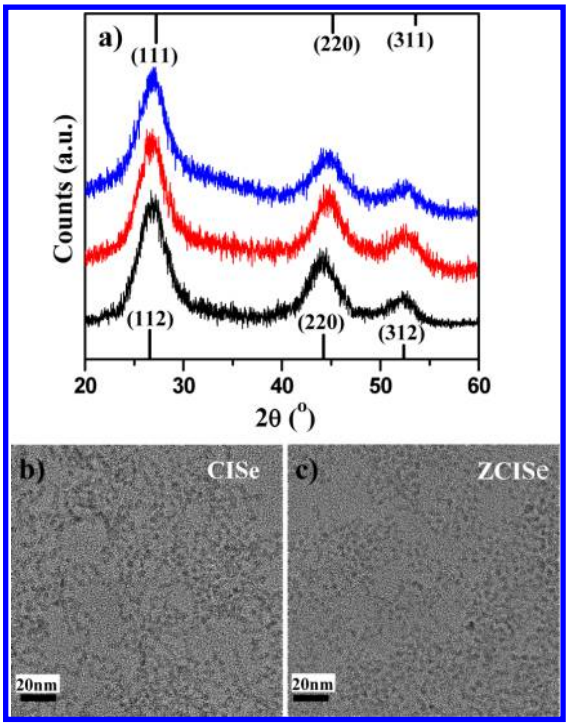

Figure 2. (a) Representative XRD patterns of Zn−Cu−In−Se QDs synthesized at 200 °C under different Zn/Cu−In ratios (black, 0; red, 0.4; blue, 0.6). Line XRD patterns correspond to bulk chalcopyrite $CuInSe_2$ (bottom), and zinc blende ZnSe (top). (b,c) TEM images of CISe and ZCISe QDs.

cells based on CISe QDs. The transmission electron microscopy (TEM) images of ZCISe and CISe QDs show that these QDs have a nearly identical average particle size of 4.1 ± 0.3 nm (Figure 2b and c). The homogeneous size distribution in TEM observation is consistent with the distinct excitonic peak observed in the absorption spectra as shown in Figure 1a and b. Furthermore, both the uniform size distribution and the small particle size of the obtained QD sensitizers favor the efficient immobilization of QDs on TiO_2 film electrode as discussed below.

Besides narrow band gap, a higher conduction band (CB) edge relative to that of TiO_2 matrix is also a prerequisite for QD sensitizers in the construction of high efficiency QDSCs.[1−5] To evaluate the effectiveness of photogenerated electron injection from ZCISe QDs to TiO_2 matrix, electronic structures of ZCISe and reference CISe QDs were measured through ultraviolet photoelectron spectroscopy (UPS) technique in combination with absorption spectra. Band gaps (E_g) and valence band (VB) edges of the studied QDs were determined through the corresponding absorption spectra (Figure 1 and Table S1) and UPS data (Figure 3a and b), respectively. The conduction band (CB) edges of the QDs were then approximated using the corresponding E_g and VB edges. The obtained energy level diagrams are illustrated in Figure 3c. It is found that the CB edges vary in an order of ZCISe > CISe > TiO_2. The higher CB edge of ZCISe corresponds to stronger driving force for electron injection from QDs into TiO_2 electron conductor and thus favors the electron injection rate.[45] This is corroborated by the greater electron injection rate as discussed below.

Transient Absorption Measurements. To unravel the influence of alloying wide band gap ZnSe with CISe host QDs

DOI: 10.1021/jacs.6b00615
J. Am. Chem. Soc. 2016, 138, 4201−4209

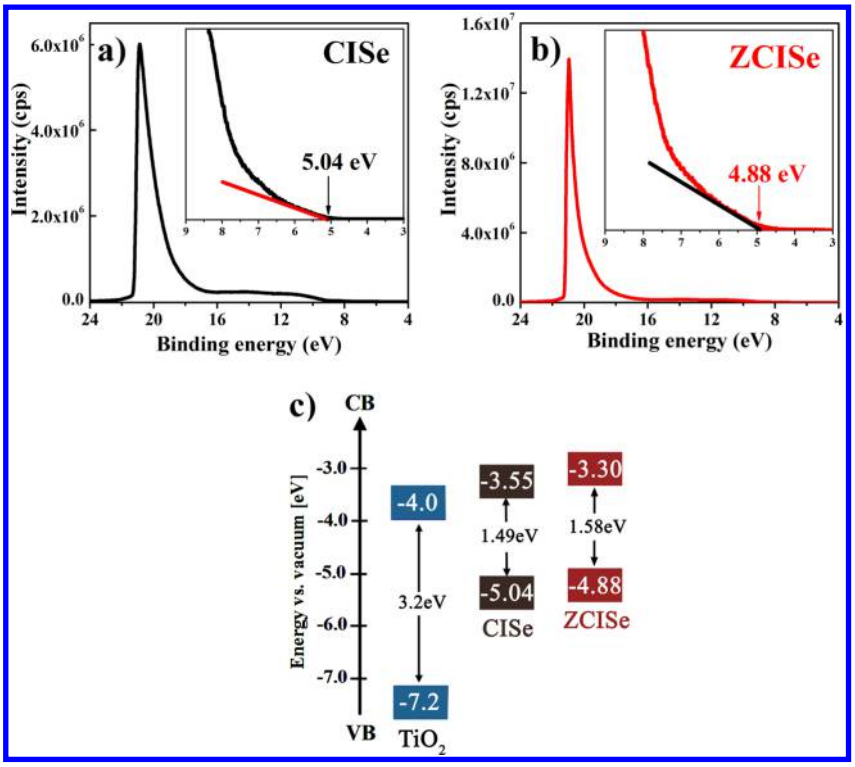

Figure 3. UPS spectra of CISe (a) and ZCISe (b) QDs. (c) Schematic energy level diagrams of TiO_2, 4.1 nm CISe, and ZCISe QDs.

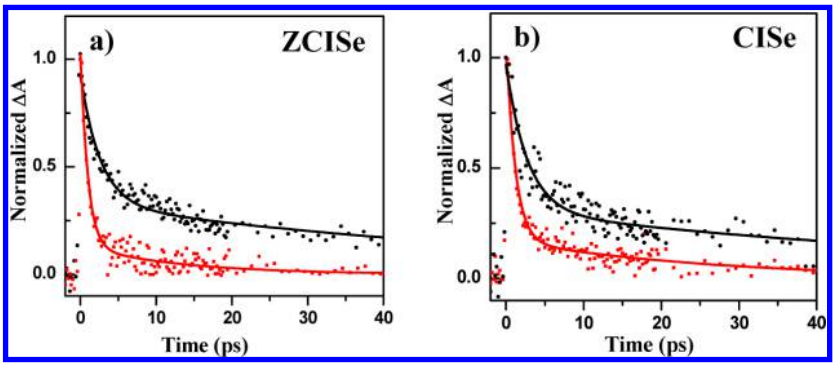

Figure 4. Transient absorption analysis. Kinetic traces of the excitonic decay of (a) ZCISe and (b) CISe QDs deposited on SiO_2 (black scatters) and TiO_2 (red scatters) substrates. Bold lines are the corresponding fitting curves.

Table 1. Fitting Results of the TA Responses, the Calculated Average Lifetime (τ_{av}), and the Electron Injection Rate (k_{et})

sample	τ_1 (ps)	τ_2 (ps)	A_1	A_2	τ_{av} (ps)	R^2	k_{et} ($\times 10^{10}$/s)
SiO_2/ZCISe	2.62 ± 0.20	61.73 ± 5.43	0.60 ± 0.02	0.33 ± 0.01	57.4	0.94	
SiO_2/CISe	2.75 ± 0.26	67.92 ± 8.95	0.66 ± 0.03	0.31 ± 0.02	62.7	0.90	
TiO_2/ZCISe	0.95 ± 0.08	13.40 ± 3.10	0.93 ± 0.04	0.13 ± 0.02	9.2	0.93	9.1
TiO_2/CISe	1.21 ± 0.07	31.61 ± 4.41	1.29 ± 0.05	0.16 ± 0.01	24.5	0.94	2.4

on the electron injection rate and photoexcited carrier dynamics, the femtosecond (fs)-resolution transient absorption (TA) measurements (Figure 4) were carried out on ZCISe and CISe QDs tethered on SiO_2 or TiO_2 substrate according to literature procedure.[23,24] In this study, all measurements were carried out in N_2 atmosphere. It was found that large TA signals were observed very clearly for all samples. From the TA decay of QDs on SiO_2 substrates, the intrinsic relaxation rate of photoexcited electrons in CB (recombination with holes in VB and/or trapping by surface states) can be determined. The TA decay of QDs on SiO_2 and TiO_2 substrates can be fitted very well by using a biexponential function of eq 1.

$$y = A_1 \exp(-t/\tau_1) + A_2 \exp(-t/\tau_2) \quad (1)$$

where τ_1, τ_2 are lifetimes and A_1, A_2 are weighted coefficients for the two exponential components, respectively. The fitting results are shown in Table 1. It is found that two relaxation processes of photoexcited electrons in both CISe QDs and ZCISe QDs on SiO_2 can be observed. The faster relaxation processes with time constants of 2−3 ps should be resulted from the trapping at surface states, while the slower relaxation process with time constants of 60−70 ps can be attributed to the recombination of electrons in CB with holes in VB. As shown in Table 1, the two intrinsic relaxation processes of

DOI: 10.1021/jacs.6b00615
J. Am. Chem. Soc. 2016, 138, 4201−4209

photoexcited electrons in CISe and ZCISe QDs are almost the same. On the other hand, as shown in Figure 4, the relaxation of photoexcited electrons in the QDs tethered on TiO_2 substrates became much faster compared with those tethered on SiO_2 substrates. The time constants of the two decay processes are listed in Table 1. The faster decay of TA signals of the QDs tethered on TiO_2 should originate from the injection of photoexcited electrons from the QDs to TiO_2, which is a well-known working principle in QDSCs. The faster decay may correspond to the electron injection process through trapping states, while the slower decay may result from the direct electron transfer from CB of QDs to the CB of TiO_2. Usually, the average lifetime (τ_{av}) of photoexcited electrons in QDs can be calculated using eq 2.

$$\tau_{av} = (A_1\tau_1^2 + A_2\tau_2^2)/(A_1\tau_1 + A_2\tau_2) \quad (2)$$

As shown in Table 1, both ZCISe and CISe QDs on insulating SiO_2 substrate show a similar average lifetime of about 60 ps. However, the average lifetime for ZCISe on TiO_2 (9.2 ps) is much smaller than that for CISe on TiO_2 (24.5 ps), indicating a remarkable decrease in the QD internal recombination (i.e recombination occurred before charge injection into TiO_2 matrix) and thus the improvement of electron injection efficiency. The corresponding electron injection rate constant k_{et} can then be calculated from eq 3.

$$k_{et} = 1/\tau_{av(TiO_2)} - 1/\tau_{av(SiO_2)} \quad (3)$$

As shown in Table 1, the obtained k_{et} for ZCISe QDs on TiO_2 is 9.1×10^{10} s^{-1}, which is almost four times larger than that for CISe QDs on TiO_2 (2.4×10^{10} s^{-1}). This result indicates that alloying ZnSe with CISe can dramatically promote the electron injection rate. This finding is in good accordance with the UPS results as discussed above, where the CB edge moves upward by alloying ZnSe with CISe, leading to the stronger driving force for electron injection from the CB of QDs into the CB of TiO_2 matrix. It should also be noted that the observed k_{et} at the level of 10^{10} s^{-1} in this work is remarkably faster than the results in previous reports.[23,24] The faster injection rate may be derived from the smaller QD size and the strong coupling between QD and TiO_2 matrix.

Although the above-mentioned calculation method for electron injection rate is commonly used in QDSC field, it should be noted that Klimov and co-workers thoughtfully investigated TA signals in QDs on TiO_2 substrates with or without electrolytes recently.[46] They suggested that the exact electron injection rate should be deduced from the TA responses measured in electrolytes rather than those measured in air or inert gas atmosphere since there may be a charging problem in the latter. In our case, we measured and compared the TA responses both on insulating SiO_2 and conductive TiO_2 substrate in N_2 atmosphere. It was found that the intrinsic photoexcited electron relaxation processes were almost the same in CISe QDs and ZCISe QDs on SiO_2, but it was very clear that the relaxation of photoexcited electrons in ZCISe QDs on TiO_2 became about four times faster than that in CISe QDs on TiO_2. If there is also a photocharging problem in our case, it means that the charging situation in CISe QDs and ZCISe QDs are quite different. The further investigation such as the measurement in electrolyte will be carried out in the future.

Assembly of QDSCs. The QD sensitized photoanodes were obtained by immobilizing MPA-capped water-soluble QDs on TiO_2 film electrode via the capping ligand-induced self-assembly approach.[47] It is worthy to note that the deposition process for both ZCISe and CISe QDs can be finished in less than 0.5 h, which is remarkably faster than the common 2−6 h for depositing other QDs with the same sensitization approach in our previous reports.[24,39,47] This should be ascribed to the relatively smaller particle size (~4 nm) of ZCISe and CISe QDs used in this work compared to the QD size of 5−6 nm in our previous work.[47] The small particle size can reduce the blocking effect for particle penetrating through the nanoscaled channels inside TiO_2 matrix and thus accelerate the immobilization of QD on TiO_2 surface. As observed previously,[24,39,47] this sensitization approach can bring forward a uniform and dense coverage of QD on TiO_2 surface as illustrated in the TEM images of QD-sensitized TiO_2 film electrodes (Figure S3). On the other hand, in order to compensate the smaller light absorption coefficient due to the smaller particle size,[48] an ~25 μm thick TiO_2 photoanode film, which is nearly double of the typical thickness in our previous reports (~15 μm),[47] was used in this work to enhance the loading amount of QD sensitizers and ensure the complete capture of sunlight. After the sensitization step, the film electrodes were then sequentially overcoated with ZnS and SiO_2 energetic barrier layers to minimize the charge recombination process occurring at the photoanode/electrolyte interfaces as previously reported.[33] Ti mesh supported mesoporous carbon electrodes (MC/Ti) were used as the counter electrode (CE). MC was synthesized via a silica template nanocasting route according to the literature.[49] MC paste was then prepared by mixing the obtained MC with ethyl cellulose in terpineol. The MC/Ti CEs were obtained by screen printing MC paste on Ti mesh substrate according to a standard procedure,[50] as presented in the Experimental Section. Complete QDSCs with a sandwich configuration were constructed by assembling the QD sensitized TiO_2 photoanodes and MC/Ti CEs with aqueous polysulfide solution containing 2.0 M S and Na_2S as the electrolyte.

Photovoltaic Performance. The current density−voltage (J−V) curves of champion ZCISe and CISe QDSCs with an active area of 0.238 cm^2 defined by black metal mask under standard condition (AM 1.5 G, 100 mW/cm^2) are shown in Figure 5a. The main photovoltaic parameters for each champion cell and the average value of five cells in each group are listed in Table 2. The detailed results for individual cells are available in Figure S4 and Table S5. It is found that all the photovoltaic parameters (short-circuit current density (J_{sc}), open-circuit voltage (V_{oc}), and fill factor (FF)) of ZCISe

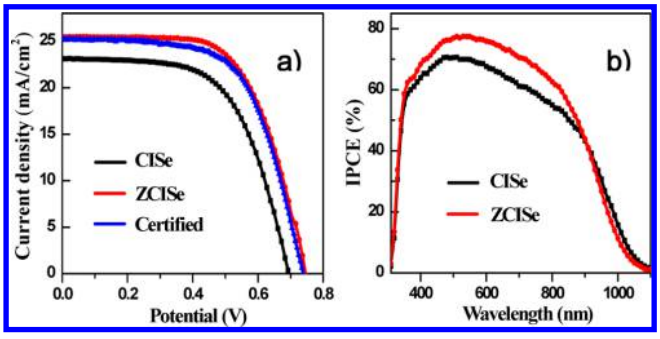

Figure 5. Photovoltaic performances of QDSCs sensitized with ZCISe and CISe QDs. (a) J−V curves for the champion cells, recorded under the standard condition (AM 1.5 G, 100 mW/cm^2). Blue curve is the certified J−V curve. (b) Corresponding IPCE spectra.

DOI: 10.1021/jacs.6b00615
J. Am. Chem. Soc. 2016, 138, 4201−4209

Table 2. Photovoltaic Parameters of QDSCs Extracted from *J*–*V* Measurements under One Full Sun Condition

cells	J_{sc} (mA/cm^2)	V_{oc} (V)	FF	PCE (%)
CISe[a]	23.00	0.689	0.602	9.54 ± 0.15
ZCISe[a]	25.18	0.742	0.624	11.66 ± 0.17
CISe[b]	23.11	0.696	0.606	9.75
ZCISe[b]	25.49	0.745	0.627	11.91
ZCISe[c]	25.25	0.739	0.622	11.61

[a]Average value from five cells prepared in parallel. [b]Performance of champion cells. [c]Certified value.

QDSCs are superior to those of CISe ones. An average PCE of 11.66 ± 0.17% has been achieved for ZCISe QDSCs, which is 22% higher than that of CISe QDSCs (9.54 ± 0.15%). The champion ZCISe QDSC provided a PCE of 11.91% (J_{sc} = 25.49 mA/cm^2, V_{oc} = 0.745 V, and FF = 0.627) and a third-party certified efficiency of 11.61% by the National Center of Supervision and Inspection on Solar Photovoltaic Products Quality of China (CPVT). Detailed information on the photovoltaic certification is available in the SI. To our knowledge, this value is the highest PCE among QD based solar cells in all configurations.[6−9] It is believed that this significant progress also pushes the performance of QDSCs to the same level of its analogue dye-sensitized solar cells (DSCs) for the first time.[51,52]

The superior efficiency of ZCISe QDSCs relative to CISe QDSCs and previously reported results is mainly derived from the high J_{sc} and V_{oc}. The high J_{sc} (25.18 mA/cm^2) should be ascribed to the broadened optoelectronic response range up to ~1100 nm as shown in the IPCE (incident photon-to-electron efficiency) spectra (Figure 5b) as well as in the absorption spectra (Figure 1b). The integrated current density based on IPCE spectra are 25.1 and 23.1 mA/cm^2 for ZCISe and CISe cells, respectively, which are perfectly consistent with the measured J_{sc} values as shown in Table 2. It is known that the optoelectronic ranges for the conventional CdSe and $CdSe_xTe_{1-x}$ QD sensitizers are less than 700 and 850 nm. This translates the best J_{sc} for CdSe and $CdSe_xTe_{1-x}$ QDSCs at the level of 16 and 21 mA/cm^2, respectively.[24,39,47] The observed higher J_{sc} for ZCISe vs CISe QDSCs (25.18 vs 23.00 mA/cm^2) can be ascribed to the faster electron injection rate as demonstrated by TA measurements. The larger k_{et} value in TA measurement can also interpret the observed higher IPCE value in ZCISe cells compared with CISe cells.

Impedance Spectroscopy Analysis. In order to reveal the intrinsic mechanism of the higher V_{oc} in ZCISe QDSCs compared to CISe QDSCs, impedance spectroscopy (IS) characterizations were performed under dark conditions to obtain the dynamic information on charge recombination and transport. IS can distinguish the electrochemical property for each part in a cell device, such as photoanode, counter electrode, and electrolyte diffusion at different forward voltage bias.[53,54] The Nyquist curves for both ZCISe and CISe cells under different bias are available in Figure S5. The corresponding IS parameters were extracted with a standard simulation circuit for QDSCs.[53,54] It has been well established that the chemical capacitance C_μ stands for the variation of electron density dependent on the Fermi level and monitors the distribution of traps states in the band gap of TiO_2 matrix. The recombination resistance R_{rec} is a measure of the charge recombination rate occurring at the photoanode/electrolyte interfaces. Its value is inversely proportional to the charge recombination rate.[53,54] The dependences of the extracted C_μ and R_{rec} on the forward bias are presented in Figure 6a and 6b, respectively. The nearly identical C_μ values for both cells as

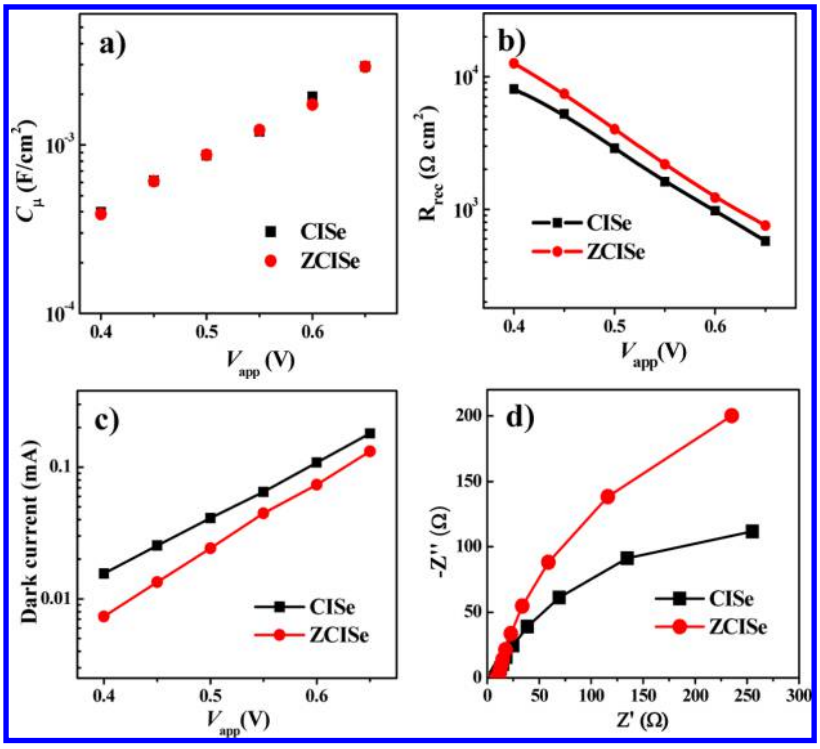

Figure 6. Impedance spectroscopy analysis of QDSCs based on ZCISe (red) and CISe (black) QD sensitizers. (a) Chemical capacitance C_μ, (b) recombination resistance R_{rec}, and (c) dark current dependent on the applied bias (V_{app}), and (d) Nyquist plots of both cells at the forward bias of −0.65 V.

DOI: 10.1021/jacs.6b00615
J. Am. Chem. Soc. 2016, 138, 4201−4209

shown in Figure 6a indicates that different QD sensitizers did not influence the conduction band edge of the TiO_2 matrix. This finding is consistent with the results in previous reports.[6,24,33] However, as shown in Figure 6b, a considerable difference in R_{rec} values was observed between the two cells. The R_{rec} values at different bias for ZCISe cells are about 2-fold higher than those of CISe cells. For clarity, Figure 6d presents a direct comparison of Nyquist plots for ZCISe and reference CISe cells at forward bias of −0.65 V, which is close to the V_{oc} values of the two cells. The extracted IS parameters are listed in Table S6. It can be found that the extracted R_{rec} value of ZCISe cells (757 $\Omega \cdot cm^2$) is more than 2-fold higher than that of CISe cells (375 $\Omega \cdot cm^2$). In addition, the electron lifetime ($\tau_n = R_{rec}C_\mu$) of the ZCISe cells at this forward bias is over 1000 ms longer than that of the CISe cells, indicating a much slower recombination rate in the ZCISe QDSCs. The notably higher R_{rec} in ZCISe vs CISe QDSCs implies that the charge recombination rate is significantly suppressed in ZCISe cells. The suppressed recombination will benefit the enhancement of photovoltaic performance, especially for V_{oc}. This conclusion is well consistent with the $J-V$ measurement results (Table 2). Meanwhile, the dark current measurement results (Figure 6c) gives further support to the suppressed recombination in ZCISe cells compared with CISe cells since all dark currents in ZCISe cells are lower than those in CISe cell at the same applied bias.

It should noted that the observed larger R_{rec} in ZCISe vs CISe QDSCs should be ascribed to the suppressed recombination occurring at TiO_2/QD or QD/electrolyte interface, but not the TiO_2/electrolyte interface. This is because the identical device configuration was adopted in both cells (i.e., identical TiO_2 film electrode, redox electrolyte, and counter electrode). There should be no difference in the recombination of photogenerated electrons at TiO_2 matrix with oxidized state species in electrolyte between two kinds of cells. As described above, the alloying process between ZnSe and CISe would harden the crystalline structure and diminish the surface trapping defects, thus suppress the recombination route starting from QD sensitizers. It should be noted that the use of MC/Ti CE instead of the conventional Cu_2S/FTO or Cu_2S/brass CE also has a contribution to the observed superior photovoltaic performance of the ZCISe QDSCs. A further investigation is underway.

In summary, new Cd-, Pb-free green Zn−Cu−In−Se QDs with tunable band gaps have been successfully developed for high efficiency QDSCs. A champion PCE of 11.91% and a certified PCE of 11.61% have been achieved, which is the best photovoltaic performance among the reported state-of-the-art QD solar cells up to date. The extraordinary PCE of ZCISe based QDSCs can be ascribed to (1) the high loading amount of QD sensitizers and broadened light-harvesting range extending to NIR window; (2) the fast electron injection rate up to 9.1×10^{10} s^{-1}; and (3) the significantly suppressed charge recombination kinetics at photoanode/electrolyte interface. These interesting findings in combination with the optimization of redox electrolyte and counter electrode would open up opportunities for developing "green" QDSCs with photovoltaic performances catching up to or even surpassing DSCs.

EXPERIMENTAL SECTION

Chemicals. Oleylamine (OAm, 95%), selenium powder (200 mesh, 99.99%), and 1-octadecene (ODE, 90%) were received from Aldrich. Diphenylphosphine (DPP, 98%) and zinc acetate ($Zn(OAc)_2$, 99.99%) were purchased from J&K. Indium acetate ($In(OAc)_3$, 99.99%), copper iodide (CuI, 99.998%), and 3-mercaptopropionic acid (MPA, 97%) were obtained from Alfa Aesar. All chemicals were used as received without further processing.

Synthesis of Cu−In−Se and Zn−Cu−In−Se QDs. The colloidal OAm-capped Cu−In−Se QDs were synthesized according to a modified literature method.[28] First, a DPP-Se precursor was obtained by mixing the Se powder (0.024 g, 0.3 mmol), DPP (0.3 mL) and OAm (0.5 mL) to form a bright yellow solution. In a typical synthetic process, CuI (19.0 mg, 0.1 mmol), $In(OAc)_3$ (29.0 mg, 0.1 mmol), OAm (2.0 mL), and ODE (2.0 mL) were loaded in a 50 mL three-necked round-bottomed flask and heated to 110 °C with stirring under vacuum for 5 min. The system was then heated to the set temperature (varying from 140 to 200 °C) followed by the injection of DPP-Se precursor prepared as above. After the injection, the reaction temperature was maintained at the set temperature for another 5 min, then cooled to 90 °C, followed by the addition of 10 mL of hexane into the reaction system. The Cu−In−Se QD dispersion was subsequently precipitated and centrifuged with the addition of excessive ethanol and acetone. OAm-capped oil-soluble Cu−In−Se QD precipitate was redissolved in dichloromethane and the ligand exchange process was then carried out with the use of MPA as phase transfer reagent to get the MPA-capped water-soluble QDs as described in our previous work.[47] The water-soluble QD precipitate was collected through precipitation and centrifugation, and then redissolved in deionized water for further use.

The oil-soluble Zn−Cu−In−Se QDs were synthesized by a method similar to that for Cu−In−Se QDs. In brief, a $Zn(OAc)_2$ stock solution was first prepared by dissolving $Zn(OAc)_2$ in a mixture of OAm and ODE with a volume ratio of 1:4. A mixture of CuI (19.0 mg, 0.1 mmol), $In(OAc)_3$ (29.0 mg, 0.1 mmol), OAm (2.0 mL), and ODE (1.5 mL) and a set amount of $Zn(OAc)_2$ stock solution (varied from 0.02 to 0.06 mmol) were heated to 200 °C, and the DPP-Se (0.3 mmol) was then injected into the reaction mixture. After reaction for 5 min, the OAm-capped Zn−Cu−In−Se QDs were collected. The water-soluble MPA-capped QDs were obtained through the same method as mentioned above for Cu−In−Se QDs.

Fabrication of Solar Cell Devices. TiO_2 mesoporous film electrodes with a thickness of 25 ± 1.5 μm (20 μm transparent layer and 5 μm light scattering layer) were prepared through screen printing method.[50] MPA-capped QD aqueous dispersion prepared as above was pipetted onto the electrodes and stands still for 0.5 h to deposit QDs. The QD sensitized photoanodes were then overcoated with ZnS passivation layers by alternately immersing the QD-sensitized photoanodes into 0.1 M Zn $(OAc)_2$ methanol solution and then 0.1 M Na_2S aqueous solution at 1 min/dip for six cycles, rinsing with distilled water between dips. After coating ZnS layer, further SiO_2 coating was performed by dipping the ZnS coated photoanodes in 0.01 M tetraethyl orthosilicate ethanol solution containing 0.1 M NH_4OH for 1 h and then rinsed with water and dried with air.

Ti mesh supported mesoporous carbon electrodes (MC/Ti) were used as counter electrodes in QDSC devices. MC was synthesized according to literature method via a silica template nanocasting route.[49] The obtained MC exhibits interconnected mesopores of ∼20 nm, specific surface area of 954 m^2 g^{-1}. The carbon pastes were made by mixing 0.1 g of MC powder and 1.0 mL of binder solution (obtained by mixing 8.0 mL of terpineol with 0.2 g of ethyl cellulose and 0.5 mL of titanium isopropoxide) and ultrasonically dispersing for 30 min. Then the MC paste was coated onto Ti mesh for preparing MC/Ti CEs via the successive screen printing technique, followed by gradually drying at 120 °C for 7 min. The screen printing process was repeated four times to obtain the optimal thickness and finally heated at 450 °C for 30 min in argon atmosphere.

Polysulfide/sulfide aqueous electrolyte was prepared by dissolving 2.0 M Na_2S and 2.0 M S in deionized water. The cell devices were constructed by assembling the counter electrodes and working electrodes in a sandwich structure with a 50 μm thick scotch tape as the spacer. In order to ensure the reliability of the evaluation data, five cells were prepared in parallel and measured under each condition.

Characterization. The UV−vis absorption and photoluminescence (PL) emission spectra were collected using a UV−visible

DOI: 10.1021/jacs.6b00615
J. Am. Chem. Soc. 2016, 138, 4201−4209

spectrophotometer (Shimadzu UV-3101 PC) and a fluorescence spectrophotometer (Cary Eclipse Varian), respectively. Transmission electron microscopy (TEM) images were obtained on a JEOL JEM-2100 microscope working at an accelerating voltage of 200 kV. Current−voltage curves ($J-V$ curves) of the QDSCs were tested using a Keithley 2400 source meter under the illumination of simulated AM 1.5G solar light (Oriel, model No. 94022A) with an intensity of 100 mW/cm^2. The light intensity was calibrated by a NREL standard Si solar cell prior to each test. No light soaking procedure was performed prior to our measurements. The voltage scan rate was set at 60 mV/s. Photoactive area of 0.238 cm^2 was defined by a black meal mask. Incident photon-to-electron conversion efficiency (IPCE) curves were measured on a Keithley 2000 multimeter under the illumination of a 300 W tungsten lamp with a Spectral Product DK240 monochromator. It should be noted that the QDSCs were usually tested 3−6 h after the assembly. It was found that without suitable package the PCE of QDSCs commonly started to degrade gradually after 2 h, and reached about 70% of their initial values over 3 h irradiation under one full sun intensity. This degradation should be mainly due to the leakage of electrolyte solution from the mesh Ti substrate used in this manuscript because the performance of the cells will recover to the initial value if new electrolyte solution was supplemented to the devices.

The transient absorption (TA) measurements were carried out in nitrogen atmosphere. A pump light with wavelength of 470 nm was used to excite the QDs and a probe wavelength of 1300 nm was used to monitor the intraband absorption of electrons from conduction band to higher excited states. The laser source is a titanium/sapphire laser (CPA-2010, Clark-MXR Inc.) with a wavelength of 775 nm, repetition rate of 1000 Hz, and pulse width of 150 fs (fs). The light was divided into two parts. One part was used to generate a white light as the probe pulse; the other as the pump light to pump an optical parametric amplifier (TOPAS from Quantronix) to generate light pulses with tunable wavelength from 290 nm to 2.3 μm. In this case, the pump light with a wavelength of 470 nm was used. All testing samples showed no apparent photodamage during the TA measurements.

Electrochemical impedance spectroscopy (EIS) characterizations were carried out on an Zennium electrochemical workstation (Zahner). EIS spectra were obtained under dark conditions at the forward bias ranging from 0.4 to 0.65 V by applying a 20 mV AC sinusoidal signal over the constant applied bias with the frequency range of 1 MHz to 0.1 Hz. The Ultraviolet Photoelectron Spectrometer (UPS) (Thermo Scientific ESCALab 250Xi) was employed to determine the valence band (VB) edges for ZCISe and CISe QDs. The chamber pressure during analysis was about 2×10^{-8} mbar. The data were acquired at −10 V bias.

■ ASSOCIATED CONTENT

Supporting Information

The Supporting Information is available free of charge on the ACS Publications website at DOI: 10.1021/jacs.6b00615.

Nominal reactant ratios and chemical compositions of ZCISe QDs prepared at 200 °C obtained by ICP-AES measurement; $J-V$ curves and photovoltaic parameters of Zn−Cu−In−Se QDs synthesized under different conditions; TEM images of CISe and ZCISe sensitized TiO_2 film electrode; certified report for photovoltaic performance of ZCISe cell; Nyquist curves under different bias voltages for both CISe and ZCISe cells (PDF)

■ AUTHOR INFORMATION

Corresponding Author

*zhongxh@ecust.edu.cn

Author Contributions

$^{\nabla}$J.D., Z.D., and J.-S.H. contributed equally.

Notes

The authors declare no competing financial interest.

■ ACKNOWLEDGMENTS

This research is supported by the Natural Science Foundation of China (Nos. 21421004, 91433106, 21573249), the Fundamental Research Funds for the Central Universities in China, and the Strategic Priority Research Program of the Chinese Academy of Sciences (Grant No. XDB12020100).

■ REFERENCES

(1) Carey, G. H.; Abdelhady, A. L.; Ning, Z.; Thon, S. M.; Bakr, O. M.; Sargent, E. H. *Chem. Rev.* **2015**, *115*, 12732−12763.
(2) Kamat, P. V. *Acc. Chem. Res.* **2012**, *45*, 1906−1915.
(3) Albero, J.; Clifford, J. N.; Palomares, E. *Coord. Chem. Rev.* **2014**, *263*, 53−64.
(4) Semonin, O. E.; Luther, J. M.; Choi, S.; Chen, H.-Y.; Gao, J.; Nozik, A. J.; Beard, M. C. *Science* **2011**, *334*, 1530−1933.
(5) Yang, J.; Choi, M. K.; Kim, D.-H.; Hyeon, T. *Adv. Mater.* **2016**, *28*, 1176−1207.
(6) Ren, Z.; Wang, J.; Pan, Z.; Zhao, K.; Zhang, H.; Li, Y.; Zhao, Y.; Mora-Sero, I.; Bisquert, J.; Zhong, X. *Chem. Mater.* **2015**, *27*, 8398−8405.
(7) Wang, J.; Li, Y.; Shen, Q.; Izuishi, T.; Pan, Z.; Zhao, K.; Zhong, X. *J. Mater. Chem. A* **2016**, *4*, 877−886.
(8) Lan, X.; Voznyy, O.; Kiani, A.; Arquer, F.; Abbas, A. S.; Kim, G.-H.; Liu, M.; Yang, Z.; Walters, G.; Xu, J.; Yuan, M.; Ning, Z.; Fan, F.; Kanjanaboos, P.; Kramer, I.; Zhitomirsky, D.; Lee, P.; Perelgut, A.; Hoogland, S.; Sargent, E. H. *Adv. Mater.* **2016**, *28*, 299−304.
(9) Kim, G.-H.; García de Arquer, F. P.; Yoon, Y. J.; Lan, X.; Liu, M.; Voznyy, O.; Yang, Z.; Fan, F.; Ip, A. H.; Kanjanaboos, P.; Hoogland, S.; Kim, J. Y.; Sargent, E. H. *Nano Lett.* **2015**, *15*, 7691−7696.
(10) Kim, M. R.; Ma, D. *J. Phys. Chem. Lett.* **2015**, *6*, 85−99.
(11) Booth, M.; Brown, A. P.; Evans, S. D.; Critchley, K. *Chem. Mater.* **2012**, *24*, 2064−2070.
(12) Leach, A. D. P.; Macdonald, J. E. *J. Phys. Chem. Lett.* **2016**, *7*, 572−583.
(13) Kuo, K. T.; Liu, D. M.; Chen, S. Y.; Lin, C. C. *J. Mater. Chem.* **2009**, *19*, 6780−6788.
(14) Chang, J.-Y.; Su, L.-F.; Li, C.-H.; Chang, C.-C.; Lin, J.-M. *Chem. Commun.* **2012**, *48*, 4848−4850.
(15) Wang, Y.; Rui, Y.; Zhang, Q.; Li, Y.; Wang, H. *ACS Appl. Mater. Interfaces* **2013**, *5*, 11858−11864.
(16) Xu, G.; Ji, S.; Miao, C.; Liu, G.; Ye, C. *J. Mater. Chem.* **2012**, *22*, 4890−4896.
(17) Chang, J. Y.; Lin, J. M.; Su, L. F.; Chang, C. F. *ACS Appl. Mater. Interfaces* **2013**, *5*, 8740−8752.
(18) Luo, J.; Wei, H.; Huang, Q.; Hu, X.; Zhao, H.; Yu, R.; Li, D.; Luo, Y.; Meng, Q. *Chem. Commun.* **2013**, *49*, 3881−3883.
(19) Hu, X.; Zhang, Q.; Huang, X.; Li, D.; Luo, Y.; Meng, Q. *J. Mater. Chem.* **2011**, *21*, 15903−15905.
(20) Li, T. L.; Lee, Y. L.; Teng, H. S. *Energy Environ. Sci.* **2012**, *5*, 5315−5324.
(21) Lin, C. Y.; Teng, C. Y.; Li, T. L.; Lee, Y. L.; Teng, H. S. *J. Mater. Chem. A* **2013**, *1*, 1155−1162.
(22) Li, T. L.; Lee, Y. L.; Teng, H. S. *J. Mater. Chem.* **2011**, *21*, 5089−5098.
(23) Santra, P. K.; Nair, P. V.; Thomas, K. G.; Kamat, P. V. *J. Phys. Chem. Lett.* **2013**, *4*, 722−729.
(24) Pan, Z.; Mora-Seró, I.; Shen, Q.; Zhang, H.; Li, Y.; Zhao, K.; Wang, J.; Zhong, X.; Bisquert, J. *J. Am. Chem. Soc.* **2014**, *136*, 9203−9210.
(25) Witt, E.; Kolny-Olesiak, J. *Chem. - Eur. J.* **2013**, *19*, 9746−9753.
(26) McDaniel, H.; Fuke, N.; Pietryga, J. M.; Klimov, V. I. *J. Phys. Chem. Lett.* **2013**, *4*, 355−361.
(27) McDaniel, H.; Fuke, N.; Makarov, N. S.; Pietryga, J. M.; Klimov, V. I. *Nat. Commun.* **2013**, *4*, 2887.

DOI: 10.1021/jacs.6b00615
J. Am. Chem. Soc. 2016, 138, 4201−4209

(28) Panthani, M. G.; Stolle, C. J.; Reid, D. K.; Rhee, D. J.; Harvey, T. B.; Akhavan, V. A.; Yu, Y.; Korgel, B. A. *J. Phys. Chem. Lett.* **2013**, *4*, 2030−2034.
(29) Panthani, M. G.; Akhavan, V.; Goodfellow, B.; Schmidtke, J. P.; Dunn, L.; Dodabalapur, A.; Barbara, P. F.; Korgel, B. A. *J. Am. Chem. Soc.* **2008**, *130*, 16770−16777.
(30) Akhavan, V. A.; Goodfellow, B. W.; Panthani, M. G.; Reid, D. K.; Hellebusch, D. J.; Adachi, T.; Korgel, B. A. *Energy Environ. Sci.* **2010**, *3*, 1600−1606.
(31) Kim, J.-Y.; Yang, J.; Yu, J.-H.; Baek, W.; Lee, C.-H.; Son, H.-J.; Hyeon, T.; Ko, M.-J. *ACS Nano* **2015**, *9*, 11286−11295.
(32) Yang, J.; Kim, J.-Y.; Yu, J. H.; Ahn, T.-Y.; Lee, H.; Choi, T.-S.; Kim, Y.-W.; Joo, J.; Ko, M. J.; Hyeon, T. *Phys. Chem. Chem. Phys.* **2013**, *15*, 20517−20525.
(33) Zhao, K.; Pan, Z.; Mora-Sero, I.; Canovas, E.; Wang, H.; Song, Y.; Gong, X.; Wang, J.; Bonn, M.; Bisquert, J.; Zhong, X. *J. Am. Chem. Soc.* **2015**, *137*, 5602−5609.
(34) Aldakov, D.; Lefrançois, A.; Reiss, P. *J. Mater. Chem. C* **2013**, *1*, 3756−3776.
(35) Hodes, G. *J. Phys. Chem. C* **2008**, *112*, 17778−17787.
(36) Li, W.; Pan, Z.; Zhong, X. *J. Mater. Chem. A* **2015**, *3*, 1649−1655.
(37) Regulacio, M. D.; Han, M.-Y. *Acc. Chem. Res.* **2010**, *43*, 621−630.
(38) Zhong, X.; Han, M.; Dong, Z.; White, T. J.; Knoll, W. *J. Am. Chem. Soc.* **2003**, *125*, 8589−8594.
(39) Pan, Z.; Zhao, K.; Wang, J.; Zhang, H.; Feng, Y.; Zhong, X. *ACS Nano* **2013**, *7*, 5215−5222.
(40) Li, L.; Pandey, A.; Werder, D. J.; Khanal, B. P.; Pietryga, J. M.; Klimov, V. I. *J. Am. Chem. Soc.* **2011**, *133*, 1176−1179.
(41) Xie, R.; Rutherford, M.; Peng, X. *J. Am. Chem. Soc.* **2009**, *131*, 5691−5697.
(42) Zhong, H.; Lo, S. S.; Mirkovic, T.; Li, Y.; Ding, Y.; Li, Y.; Scholes, G. D. *ACS Nano* **2010**, *4*, 5253−5262.
(43) Chen, B.; Zhong, H.; Zhang, W.; Tan, Z.; Li, Y.; Yu, C.; Zhai, T.; Bando, Y.; Yang, S.; Zou, B. *Adv. Funct. Mater.* **2012**, *22*, 2081−2088.
(44) Chang, C. C.; Chen, J. K.; Chen, C. P.; Yang, C. H.; Chang, J. Y. *ACS Appl. Mater. Interfaces* **2013**, *5*, 11296−11306.
(45) Robel, I.; Kuno, M.; Kamat, P. V. *J. Am. Chem. Soc.* **2007**, *129*, 4136−4137.
(46) Makarov, N. S.; McDaniel, H.; Fuke, N.; Robel, I.; Klimov, V. I. *J. Phys. Chem. Lett.* **2014**, *5*, 111−118.
(47) Li, W.; Zhong, X. *J. Phys. Chem. Lett.* **2015**, *6*, 796−806.
(48) Yu, W. W.; Qu, L.; Guo, W.; Peng, X. *Chem. Mater.* **2003**, *15*, 2854−2860.
(49) Chen, H.; Sun, F.; Wang, J.; Li, W.; Qiao, W.; Ling, L.; Long, D. *J. Phys. Chem. C* **2013**, *117*, 8318−8328.
(50) Ito, S.; Murakami, T. N.; Comte, P.; Liska, P.; Grätzel, C.; Nazeeruddin, M. K.; Grätzel, M. *Thin Solid Films* **2008**, *516*, 4613−4619.
(51) Yella, A.; Lee, H.-W.; Tsao, H. N.; Yi, C.; Chandiran, A. K.; Nazeeruddin, M.K.; Diau, E. W.; Yeh, C.-Y.; Zakeeruddin, S. M.; Grätzel, M. *Science* **2011**, *334*, 629−634.
(52) Mathew, S.; Yella, A.; Gao, P.; Humphry-Baker, R.; Curchod, B. F. E.; Ashari-Astani, N.; Tavernelli, I.; Rothlisberger, U.; Nazeeruddin, M. K.; Grätzel, M. *Nat. Chem.* **2014**, *6*, 242−247.
(53) González-Pedro, V.; Xu, X.; Mora-Seró, I.; Bisquert, J. *ACS Nano* **2010**, *4*, 5783−5790.
(54) Fabregat-Santiago, F.; Garcia-Belmonte, G.; Mora-Seró, I.; Bisquert, J. *Phys. Chem. Chem. Phys.* **2011**, *13*, 9083−9118.

DOI: 10.1021/jacs.6b00615
J. Am. Chem. Soc. 2016, 138, 4201−4209